CHEMISTRY OF MATERIALS

Article

pubs.acs.org/cm

Reproducible One-Step Fabrication of Compact $MAPbI_{3-x}Cl_x$ Thin Films Derived from Mixed-Lead-Halide Precursors

Dong Wang,[†,‡] Zhihong Liu,[†,‡] Zhongmin Zhou,[†] Huimin Zhu,[§] Yuanyuan Zhou,[⊥] Changshui Huang,[†] Zaiwei Wang,[†] Hongxia Xu,[†] Yizheng Jin,[∥] Bin Fan,[#] Shuping Pang,*[,†] and Guanglei Cui*[,†]

[†]Qingdao Institute of Bioenergy and Bioprocess Technology, Chinese Academy of Sciences, Qingdao 266101, P.R. China

[§]Qingdao University of Science and Technology, Qingdao 266042, P.R. China

[⊥]School of Engineering, Brown University, Providence, Rhode Island 02912, United States

[∥]Zhejiang University, Hangzhou 310027, P.R. China

[#]Weihua Solar Co. Ltd., Xiamen 361115, P.R. China

Supporting Information

ABSTRACT: Methylammonium lead trihalide perovskites are attracting intensive interest due to its high photovoltaic performance, low cost and one-step solution processability. Since the morphology of the perovskite thin films play the central role on the cell performance, a plethora of methods have been developed to fabricate uniform perovskite film. Herein, we demonstrate that an innovative approach by applying mixed lead salts (PbI_2 + $PbCl_2$) to facilitate reproducible fabrication of compact perovskite thin film. It is proposed that rapid reaction kinetics of PbI_2 with MAI enables preformation of perovskite within the intermidiate film matrix, working as homogeneously located domains for squential growth of the $PbCl_2$-derived perovskite. The as-prepared perovskite film exhibited a overall textured crystal morphology and superior compactness, which enables excellent light absorption and long-time preservation of photogenerated charge carriers and therefore exhibits 11% efficiency in planar-structured solar cells. The annealing testing shows the film also possesses very stable morphology upon long-time heating, indicative of the insensitivity of our new protocol to the preparation condition and also the promising thermal stability of its based solar cells. The simplicity of the one-step solution-processing and the high morphology stability of the as-prepared perovskite film endow this mixing lead salts method with feasibility of the large-scale fabrication.

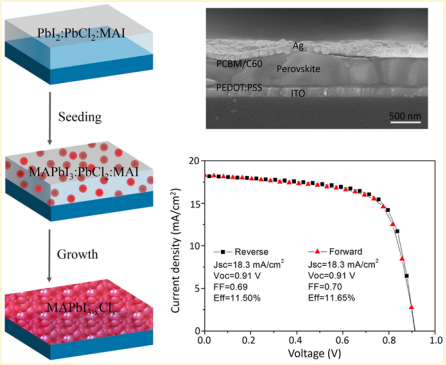

1. INTRODUCTION

Methylammonium lead tri-iodide ($CH_3NH_3PbI_3$, $MAPbI_3$) emerges as a new "game-player" in the field of photovoltaic cells because of their excellent electronic properties and versatility of deposition methods.[1−4] Recent progress with more than 16% power conversion efficiency (PCE) in either a mesoscopic cell or a planar heterojunction cell has been demonstrated by improving film processing and optimizing device architectures.[5−9] The planar heterojunction cells, where the perovskite film is sandwiched between the hole and electron selective contacts, have simpler architecture and can be fabricated at relatively low temperature.[3,10−17] To realize high-efficiency planar perovskite solar cells, it has been ambiguously shown that the morphology of the perovskite film is one of the most essential factors affecting the photovoltaic parameters.[18,19] Various deposition techniques have been reported to fabricate perovskite thin films, including one-step spin-coating process-ing,[20−22] in situ dipping method,[23,24] vapor deposition,[25,26] and vapor−solution hybrid deposition.[27] To meet the commercial requirement of high throughput manufacturing processes, the one-step solution processing followed by thermal annealing is the most promising and universal method considering its compatibility of roll-to-roll mass production on the flexible substrate.

For typical one-step solution-processing of perovskite film, two types of precursor solutions are applied based on selection of Pb halides (PbI_2 or $PbCl_2$). One is using the mixture of PbI_2 and methylammonium iodide (MAI) with a mole ratio of 1:1 (denoted as PbI_2 based method here), which produce a polycrystalline $MAPbI_3$ perovskite film, and the other is employing $PbCl_2$ and MAI with a molar ratio of 1:3 (denoted as $PbCl_2$-based method here), which results in a highly textured $MAPbI_{3-x}Cl_x$ perovskite film with negligible amount of chorine inclusion.[28] Based on these methods, lots of efforts have been done in order to produce perovskite thin film with improved coverage which reduces detrimental contact between electron selecting layer and hole extracting layer. Such efforts include controlling the annealing condition,[18] using mixed solvents,[29] adjusting the organic/inorganic component ratio,[13,30] adding additives in the solution,[31,32] and very recently, reported solvent

Received: October 15, 2014
Revised: November 23, 2014
Published: November 24, 2014

engineering,[6,9] etc. Although these protocols show improvements in the film formation and the photovoltaic performance as well, reproducible fabrication of highly homogeneous and morphological stable perovskite films with a simple route beyond the laboratory scale is highly demanded.

In this study, we developed a simple one-step solution processing method by using the mixed lead salts (PbI_2 and $PbCl_2$, denoted as ML method) to control the crystallization process, which enabled full coverage $MAPbI_{3-x}Cl_x$ film. Note that, the formula $MAPbI_{3-x}Cl_x$ is used in this text once the chlorine is involved in the perovskite formation reaction. It is demonstrated that the rapid reaction of MAI with PbI_2 in the precursors contributes preformed perovskite crystallite domains for sequential perovskite film growth and the overall formation rate of perovskite is tailed by PbI_2:$PbCl_2$ ration in the precursor solution. The optimized $MAPbI_{3-x}Cl_x$ film with preferred lattice orientation and compact nature exhibits high absorption of light and long-time preservation of photogenerated charge carriers. Further, regardless of the textured crystal nature of $MAPbI_{3-x}Cl_x$, the as-fabricated film still exhibits a stable morphology upon long-time annealing, which indicates that the present protocol is insensitive to the thermal annealing condition and such film will contribute an outstanding thermally stable photovoltaic performance.

2. EXPERIMENTAL SECTION

2.1. Material Synthesis and Characterization. MAI and TiO_2 gel were both synthesized in the lab as we previously reported.[24] A field-emission scanning electron microscope (Hitachi S-4800) was used to acquire SEM images. X-ray diffraction (XRD) spectra were obtained from perovskite film, using a Bruker D8 advance X-ray diffractometer. An atomic force microscopy (Agilent 5400AFM) was used to analyze the surface morphology of the perovskite film. Ultraviolet spectrometer (Hitachi U-4100) was used to acquire UV spectrum. Time-resolved PL measurements were acquired using an Edinburgh Instruments FLS 920 fluorescence spectrometer. The TEM image was obtained using TEM (2100F, JEOL) operated at 200 kV accelerating voltage.

2.2. Solar Cell Fabrication and Characterization. Patterned indium−tin oxide (ITO) coated glasses were ultrasonic cleaned with deionized water, acetone, and ethanol, and dried with clean dry air. The substrate was then treated with UV/O_3 for 10 min. Subsequently, ∼40 nm thick PEDOT:PSS layer was fabricated by spin-casting, followed by a heating treatment at 150 °C for 30 min in air. Then the PEDOT:PSS covered ITO substrates were transferred to a glovebox for the following device fabrication and testing. Thin $MAPbI_3$ perovskite layer was formed by spin-casting 40 wt % PbI_2:$PbCl_2$:MAI mixture in N,N-dimethylformamide (DMF), followed by a heating treatment at 100 °C for 1 h. To get a high uniform and pure $MAPbI_{3-x}Cl_x$ perovskite phase, the mole ratio of PbI_2:$PbCl_2$:MAI mixture was modified to 1:1:4. The thickness of the perovskite films was controlled at ∼300 nm by spin coating the 40% solution at 4000 rpm. For the electron transport material, 10 mg/mL $PC_{60}BM$ dissolved in 1,2-dichlorobenzene solution was first casted onto the perovskite film and then 40 nm thick C_{60} layer was evaporated on it. Finally, 80 nm Ag electrodes were deposited by thermal-evaporation to complete the solar cells. For comparison, the precursor PbI_2:$PbCl_2$ = 2:1 and 1:2 are also used to produce perovskite solar cells with the same condition as described above. *J*−*V* characteristics were measured (2400 Series Source Meter, Keithley Instruments) in a glovebox under simulated AM 1.5G sunlight at 100 mW/cm^2. The area of the perovskite solar cells were typically 0.09 cm^2.

3. RESULTS AND DISCUSSION

The proposed ML method was illustrated in Figure 1A. First, the mixture of PbI_2/$PbCl_2$/MAI with a mole ratio of 1:1:4 was spin-coated on the glass substrate and then thermally annealed at 100 °C for 1 h. Reaction 3 associated with the formation of the perovskites can be described as reaction 1 followed by reaction 2.

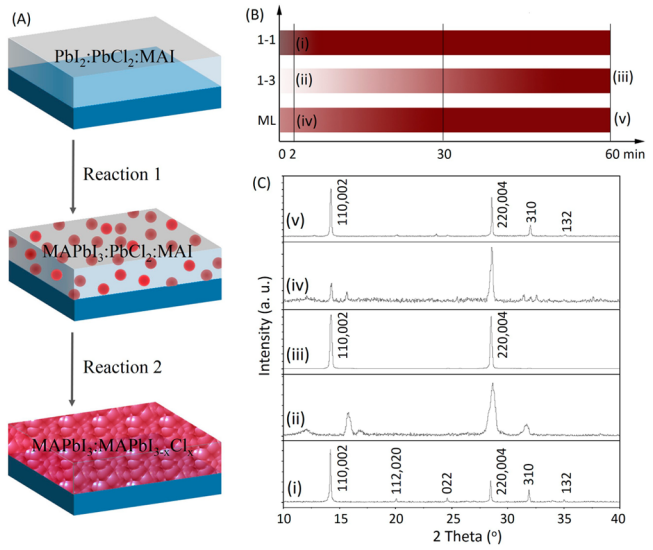

Figure 1. (A) Schematic illustration of the formation of the highly uniform perovskite film by using the mixed lead salts. (B) Comparison of the color evolution of the perovskite films along the thermal annealing treatment prepared by the PbI_2-based (1−1), $PbCl_2$-based (1−3), and ML methods, respectively. (C) XRD patterns of the perovskite films prepared with different methods and annealed with different period as labeled shown in B. Note that the samples (ii) and (iv) are very sensitive to the humidity and must be kept in a self-made Ar-filled box during the measurement.

$$PbI_2 + MAI \rightarrow MAPbI_3 \quad (1)$$

$$PbCl_2 + 3MAI \rightarrow MAPbI_{3-x}Cl_x + 2MA(g) + (2 - x)HCl(g) + xHI(g) \quad (2)$$

$$MAPbI_3 + PbCl_2 + 3MAI \rightarrow 2MAPbI_{3-x}Cl_x + 2MA(g) + (2 - 2x)HCl(g) + 2xHI(g) \quad (3)$$

It has been widely recognized that PbI_2 with MAI is more reactive than $PbCl_2$.[33] Such difference in the reaction kinetics between MAI and PbI_2 or $PbCl_2$ could be reflected by the color evolution (illustrated in Figure 1B on the basis of the UV measurement) and their corresponding XRD characterization (Figure 1C) during the thermal annealing treatment. For the traditional PbI_2 based method, the color of the as-spun film is light brown and it changed to dark immediately in seconds when the substrate was heated at 100 °C (Reaction 1). The corresponding XRD pattern in Figure 1C(i) indicates the film has been totally converted to $MAPbI_3$ perovskite at the beginning stage of the thermal annealing treatment. For the traditional $PbCl_2$ based method, the color evolution is much slower (Figure 1B, 1−3). It has been identified that the byproduct MACl in Reaction 2 could dramatically retard the formation of $MAPbI_{3-x}Cl_x$ perovskite, and the reaction moves forward with MACl evaporated or sublimed.[32] The XRD pattern shown in Figure 1C(ii) indicates that, at the beginning stage (2 min), perovskite phase was absent and only the

dx.doi.org/10.1021/cm5037869 | Chem. Mater. 2014, 26, 7145−7150

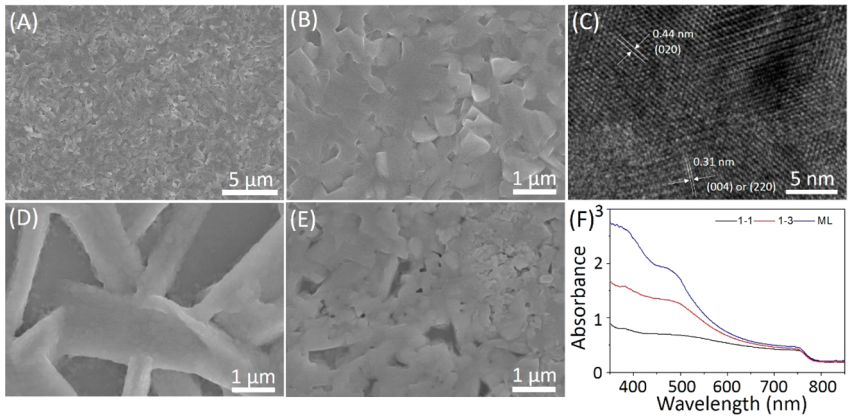

Figure 2. (A, B) SEM images and (C) HRTEM image of the perovskite films prepared by the ML method, (D, E) SEM images of the perovskite film prepared by traditional 1−1 method, and 1−3 methods, respectively. (F) Comparison of the UV−vis absorbance of the perovskite films prepared by the above three methods.

possible intermediate compound $PbCl_2{\cdot}xMAI$ exists. It took more than 45 min to form a phase-pure $MAPbI_{3-x}Cl_x$ perovskite film upon heating at 100 °C (Figure 1C(iii)). Although perovskite films produced from Reaction 2 generally show much improved coverage compared with Reaction 1, it turns out that the ultraslow process of reaction crystallization process results in large domain formation, which is responsible for the pinhole formation.

The very distinct reaction kinetics of reactions 1 and 2 enable the possibility to engineer the perovskite formation reactions by employing both PbI_2 and $PbCl_2$ as inorganic precursors (Figure S1). It is expected that reaction 1 between MAI and PbI_2 can rapidly conduct, forming homogeneously dispersed $MAPbI_3$ perovskite crystallites in the composite film matrix. This process is assumed to complete in minutes, which is similar to the PbI_2-based method. Subsequently, upon annealing, reaction 2 becomes prominent to further grow $MAPbI_{3-x}Cl_x$ perovskite from or between the preformed perovskite crystallites. To unravel the formation process, the XRD pattern at 2 min heating is shown in Figure 1C(iv). The characteristic (110) peak of perovskite at 14.1° evolves at this stage, which is indicative of the preformed $MAPbI_3$ perovskite. The peak also appears to be more broad than that in Figure 1C(i), which implies the crystal size of the preformed perovskite crystallites from Reaction 1 is much smaller than the traditional PbI_2 based method. With the subsequent heating, the color of the film turns dark in a faster rate compared with $PbCl_2$-based method, reflecting that the growth of $MAPbI_{3-x}Cl_x$ becomes accelerated because of the presence of the preformed $MAPbI_3$ crystallites.

As expected, the ML film is extremely uniform and no pinholes or void defects were found (shown in Figure 2A, B). The perovskite domain size is about 200−500 nm. The HRTEM image of the ML film shown in Figure 2C indicates its good crystallinity. In comparison, the morphologies of the perovskite films prepared by the traditional PbI_2 and $PbCl_2$ based methods were also presented in Figure 2D, E. The PbI_2-based method with DMF as the solvent delivers a bulk dendrite-like structure (Figure 2D). Compared with the PbI_2-based method, the uniformity could be obviously improved by using the $PbCl_2$ based method (Figure 2E). Nevertheless, it is widely shown that the formation of such film is sensitive to the thermal annealing condition (time, temperature, etc.),[34] This is mostly related to the highly textured film characteristic of pure $PbCl_2$ derived $MAPbI_{3-x}Cl_x$. Promisingly, our ML-method produced thin film exhibits a void-free $MAPbI_{3-x}Cl_x$ film over large area with relatively less-textured characteristics.

Figure 2F is the UV−vis absorbance spectra of the perovskite films prepared by the ML, PbI_2 and $PbCl_2$ based methods, respectively. All these films show roughly the same absorption edge at about 780 nm as shown in Figure S2 in the Supporting Information, which represents a general feature in both $MAPbI_3$ and $MAPbI_{3-x}Cl_x$.[35] The absorbance of the ML film at 500 nm is two times higher than that of the PbI_2-based film and 45% higher than that of the $PbCl_2$-based film under the same spin-coating condition. Given the absorption coefficient of $MAPbI_3$ of $\sim 1 \times 10^5$ cm^{-1} at 550 nm, it is theoretically calculated from the Beer−Lambert law $A = \lg(1/T)$ that ~300 nm thick ML perovskite film is enough to effectively absorb the visible region of light spectrum.[36]

The surface morphology of the ML perovskite film was characterized by the AFM measurement. Figure 3A is the AFM image of the top surface of the as-deposited perovskite thin film, which is similar to the SEM result in Figure 2A, B. The

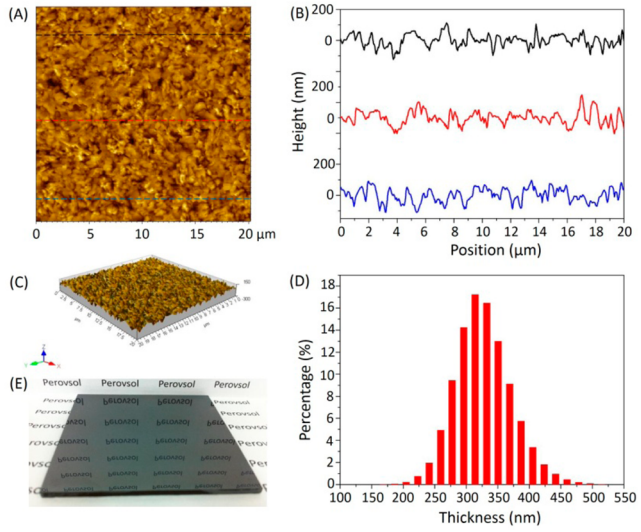

Figure 3. (A) AFM height image of the ML perovskite film. (B) Height profile along the lines drawn in A. (C) 3D AFM image of the perovskite film. (D) Thickness distribution histogram of the ML perovskite film. (E) Optical image of a perovskite film prepared by the ML method on a 5 cm × 5 cm substrate.

dx.doi.org/10.1021/cm5037869 | *Chem. Mater.* 2014, 26, 7145−7150

local surface topography data reveals a root-mean-square (RMS) roughness (20 μm × 20 μm) of only 41 nm. Together with the cross-section image of the perovskite films (not shown here), a thickness distribution histogram is drawn in Figure 3D, showing a relatively narrow thickness distribution.

To elucidate the role of the reaction rate on the morphology of the perovskite films, we tailed the mole ratio of PbI_2 to $PbCl_2$. The fraction of the preformed $MAPbI_3$ in the matrix film could be reflected by the color of the initial film as shown in Figure S3 in the Supporting Information. Figure 4A is the SEM image of the perovskite film prepared from a 40 wt % PbI_2-$PbCl_2$-MAI solution in DMF with a mole ratio of PbI_2 to $PbCl_2$ of 2:1. The perovskite film appears to be composed of large perovskite domains with more obvious boundaries compared the sample shown in Figure 2A, B. When the fraction of the added $PbCl_2$ is increased, some pinholes appear in the final perovskite film, getting close to perovskite films produced from the $PbCl_2$-based method. The XRD patterns also show a more textured film with higher preferred orientation is produced with more fraction of $PbCl_2$ added, which is consistent with the corresponding crystal morphology characteristics of $MAPbI_3$ (from reaction 1) and $MAPbI_{3-x}Cl_x$ (from reaction 2).[1,37] Such trend reveals that the combination of reactions 1 and 2 is essential for formation of pinhole-free perovskite films.

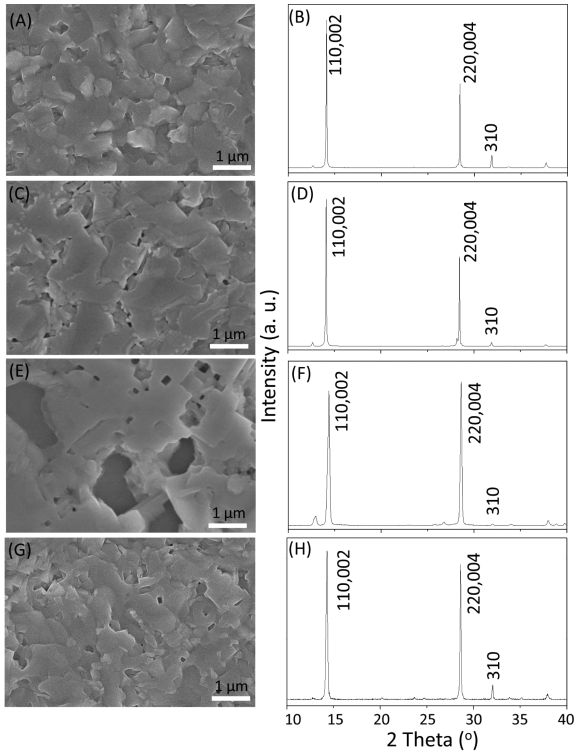

Figure 4. SEM images and corresponding XRD patterns prepared by different methods or varied thermally annealing time. The perovskite films fabricated by the ML method with the mole ratio of PbI_2 to $PbCl_2$ is of (A, B) 2:1, (C, D) 1:2. (E, F) Perovskite film prepared by $PbCl_2$ based method and annealed at 100 °C for 5 h. (G, H) ML film annealed at 100 °C for 5 h.

Besides the improved uniformity, the ML method also endow the perovskite films a promising morphological stability at high temperature. It has been demonstrated that the morphology of the perovskite film by the $PbCl_2$-based method was very sensitive to the annealing temperature and the time.[34] Figure 4E is the SEM image of the perovskite film on an ITO/PEDOT:PSS surface heated for 5 h in a glovebox. Compared with the sample heated at 100 °C for 1 h shown in Figure 2E, void defects becomes larger due to the rearrangement of the perovskite crystals, resulting in a relatively low coverage. However, based on the ML method, there is no obvious morphology change when the sample heated at 100 °C for 5 h as shown in Figure 4G. The enhanced morphological stability under high temperature was mostly related to the relatively less textured crystals in the void-free film. It has been widely shown that pure $PbCl_2$-derived $MAPbI_{3-x}Cl_x$ perovskite films are composed of laterally grown big crystal with extremely strong texture along (110) in Figure 1C(iii). Upon long time thermal annealing, such morphology was not stable and tends to evolve to a less textured morphology to reduce its surface energy as evidenced by the evolution of the (310) peak in Figure 4F. In the ML method, because the preformed $MAPbI_3$ crystallites are exhibited to be randomly oriented, the final perovskite film possesses a relatively weaker lattice texture orientation as shown in Figure 1C(v) with relatively strong (310) peak intensity although the $PbCl_2$ are involved in the growth Reaction 2. Further increase the thermally annealing time could not change the intensity of the (310) peak of the ML film as shown in Figure 4H. The effect of the preformed $MAPbI_3$ crystallites on the orientation of the perovskite film was also proved when more PbI_2 were added in the precursor solution. As shown in Figure 4B, D, the more PbI_2 existed in the precursor, the stronger relative intensity of the (310) peak.

The optical characteristics of the ML film were further characterized by the steady-state PL spectrum (Figure 5A) and time-resolved PL spectrum (Figure 5B). The peak of the PL spectra of 772 nm shows negligible Stokes shift, indicative of little vibronic relaxation of the ML film.[38] The linear fit of the PL emission edge for the pure ML film is 1.54 eV (inset in Figure 5A), which is close to the reported band gap for $MAPbI_3$.[40] The time-resolved PL characterization of the ML perovskite film is shown in Figure 5B, extremely long carrier lifetimes of τ_1 = 253 ns, τ_2 = 598 ns were observed, which are comparable to the value found in $MAPbI_{3-x}Cl_x$.[39,41] With such perovskite film, planar ITO/PEDOT:PSS/Perovskite/PCBM/C_{60}/Ag solar cells were constructed and studied. The inset in Figure 5C illustrates the planar device structure and a cross-sectional SEM image of the solar cell device. The ~300 nm thick perovskite film appears extremely dense. The typical photovoltaic parameters of these cells measured under simulated AM 1.5 G illumination at an intensity of 100 mW cm^{-2} is shown in Figure 5C. The cells exhibit an average efficiency of 11% with negligible hysteresis from both scanning directions (0.2 mV/s). Fifty cells fabricated under the same condition were made to study the reproducibility of this ML method, the efficiencies show an small relative standard derivation of ±2.2% as shown in Figure 5D.

4. CONCLUSIONS

In summary, we described an effective method to engineer the formation reaction of the perovskite by using the mixture of PbI_2 and $PbCl_2$ as lead precursors, which significantly enhanced film uniformity. A combination of XRD and annealing testing indicated that the as-prepared perovskite film also exhibits a dramatic morphological stability upon high temperature. We elucidate that the control over formation reaction rate by tuning the $PbI_2/PbCl_2$ ratio in the precursor solution plays essential role in the realization of full coverage perovskite film

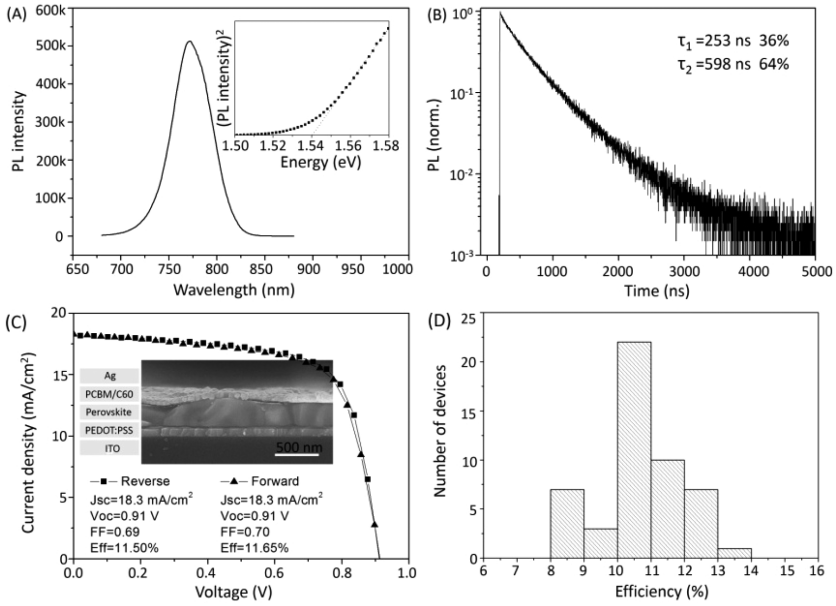

Figure 5. (A) Photoluminescence (PL) spectra of a 200 nm thick layer of ML film on a glass substrate covered with PMMA; the inset in A is its linear fit of the emission edge. (B) Time-resolved PL measurements taken at the peak emission wavelength. (C) Current density−voltage (J−V) characteristics of the solar cell measured under AM1.5 simulated sun light with a scan rate of 0.1 V s^{-1} for a device for both scanning directions. Insets are the detailed performance parameters. The inset in C is the structure and cross-sectional SEM image of the hybrid planar ITO/PEDOT:PSS/perovskite/PCBM/C60/Ag solar cell prepared by the ML method using 40 wt % perovskite solution. (D) Histograms of device efficiency measured for 50 separate perovskite solar cells with same perovskite thickness.

and the morphological stability. As regard to the photovoltaic performance of the resultant film, very reproducible PCEs with an average value of 11% were achieved in planar ITO/PEDOT:PSS/perovskite/PCBM/C60/Ag solar cells. The simplicity of the one-step solution processing and the high stability of the as-prepared perovskite film endow the ML protocol with feasibility of the large-scale fabrication.

■ ASSOCIATED CONTENT

Ⓢ Supporting Information

Optical images of the perovskite film heated for different time; UV−vis absorption of the perovskite films prepared by the 1−1, 1−3, and ML methods; UV−vis absorption of the perovskite films prepared by precursors contained different ratio of PbI_2 at different annealing stages; the parameters of solar cells fabricated by different methods. This material is available free of charge via the Internet at http://pubs.acs.org.

■ AUTHOR INFORMATION

Corresponding Authors

*E-mail: pangsp@qibebt.ac.cn.
*E-mail: cuigl@qibebt.ac.cn.

Author Contributions

‡D.W. and Z.L. contributed equally. All authors have given approval to the final version of the manuscript.

Funding

This work was financially supported by the Chinese National Natural Science Foundation (Grant 51202266, 21202178), Natural Science Foundation of Shandong Province (ZR2013FZ001), the Research Program of Qingdao (13-1-4-228-jch, 14-2-4-8-jch).

Notes

The authors declare no competing financial interest.

■ REFERENCES

(1) Docampo, P.; Guldin, S.; Leijtens, T.; Noel, N. K.; Steiner, U.; Snaith, H. J. *Adv. Mater.* **2014**, *26*, 4013−4030.
(2) Hodes, G.; Cahen, D. *Nature Photon* **2014**, *8*, 87−88.
(3) Park, N.-G. *J. Phys. Chem. Lett.* **2013**, *4*, 2423−2429.
(4) Pellet, N.; Gao, P.; Gregori, G.; Yang, T. Y.; Nazeeruddin, M. K.; Maier, J.; Gratzel, M. *Angew. Chem.* **2014**, *53*, 3151−3157.
(5) Zhou, H.; Chen, Q.; Li, G.; Luo, S.; Song, T. B.; Duan, H. S.; Hong, Z.; You, J.; Liu, Y.; Yang, Y. *Science* **2014**, *345*, 542−546.
(6) Jeon, N. J.; Noh, J. H.; Kim, Y. C.; Yang, W. S.; Ryu, S.; Seok, S. I. *Nat. Mater.* **2014**, *13*, 897−903.
(7) Chiang, C.-H.; Tseng, Z.-L.; Wu, C.-G. *J. Mater. Chem. A* **2014**, *2*, 15897−15903.
(8) Gao, P.; Gratzel, M.; Nazeeruddin, M. K. *Energy Environ. Sci.* **2014**, *7*, 2448−2463.
(9) Xiao, M.; Huang, F.; Huang, W.; Dkhissi, Y.; Zhu, Y.; Etheridge, J.; Gray-Weale, A.; Bach, U.; Cheng, Y. B.; Spiccia, L. *Angew. Chem.* **2014**, *53*, 9898−9903.
(10) Wojciechowski, K.; Saliba, M.; Leijtens, T.; Abate, A.; Snaith, H. J. *Energy Environ. Sci.* **2014**, *7*, 1142−1147.
(11) Sun, S.; Salim, T.; Mathews, N.; Duchamp, M.; Boothroyd, C.; Xing, G.; Sum, T. C.; Lam, Y. M. *Energy Environ. Sci.* **2014**, *7*, 399−407.
(12) Jeng, J. Y.; Chiang, Y. F.; Lee, M. H.; Peng, S. R.; Guo, T. F.; Chen, P.; Wen, T. C. *Adv. Mater.* **2013**, *25*, 3727−3732.
(13) Wang, Q.; Shao, Y.; Dong, Q.; Xiao, Z.; Yuan, Y.; Huang, J. *Energy Environ. Sci.* **2014**, *7*, 2359−2365.
(14) Chen, H.; Pan, X.; Liu, W.; Cai, M.; Kou, D.; Huo, Z.; Fang, X.; Dai, S. *Chem. Commun.* **2013**, *49*, 7277−7279.
(15) Conings, B.; Baeten, L.; De Dobbelaere, C.; D'Haen, J.; Manca, J.; Boyen, H. G. *Adv. Mater.* **2014**, *26*, 2041−2046.
(16) He, M.; Zheng, D.; Wang, M.; Lin, C.; Lin, Z. *J. Mater. Chem. A* **2014**, *2*, 5994−6003.
(17) Kumar, M. H.; Yantara, N.; Dharani, S.; Graetzel, M.; Mhaisalkar, S.; Boix, P. P.; Mathews, N. *Chem. Commun.* **2013**, *49*, 11089−11091.
(18) Dualeh, A.; Tétreault, N.; Moehl, T.; Gao, P.; Nazeeruddin, M. K.; Grätzel, M. *Adv. Funct. Mater.* **2014**, *24*, 3250−3258.

(19) Gonzalez-Pedro, V.; Juarez-Perez, E. J.; Arsyad, W. S.; Barea, E. M.; Fabregat-Santiago, F.; Mora-Sero, I.; Bisquert, J. *Nano Lett.* **2014**, *14*, 888−8893.
(20) Kim, H. S.; Lee, C. R.; Im, J. H.; Lee, K. B.; Moehl, T.; Marchioro, A.; Moon, S. J.; Humphry-Baker, R.; Yum, J. H.; Moser, J. E.; Gratzel, M.; Park, N. G. *Sci. Rep.* **2012**, *2*, 591−597.
(21) Lee, M. M.; Teuscher, J.; Miyasaka, T.; Murakami, T. N.; Snaith, H. J. *Science* **2012**, *338*, 643−647.
(22) Lv, S.; Pang, S.; Zhou, Y.; Padture, N. P.; Hu, H.; Wang, L.; Zhou, X.; Zhu, H.; Zhang, L.; Huang, C.; Cui, G. *Phys. Chem. Chem. Phys.* **2014**, *16*, 19206−19211.
(23) Burschka, J.; Pellet, N.; Moon, S. J.; Humphry-Baker, R.; Gao, P.; Nazeeruddin, M. K.; Gratzel, M. *Nature* **2013**, *499*, 316−319.
(24) Pang, S.; Hu, H.; Zhang, J.; Lv, S.; Yu, Y.; Wei, F.; Qin, T.; Xu, H.; Liu, Z.; Cui, G. *Chem. Mater.* **2014**, *26*, 1485−1491.
(25) Liu, M.; Johnston, M. B.; Snaith, H. J. *Nature* **2013**, *501*, 395−398.
(26) Hu, H.; Wang, D.; Zhou, Y.; Zhang, J.; Lv, S.; Pang, S.; Chen, X.; Liu, Z.; Padture, N. P.; Cui, G. *RSC Adv.* **2014**, *4*, 28964−28967.
(27) Chen, Q.; Zhou, H.; Hong, Z.; Luo, S.; Duan, H. S.; Wang, H. H.; Liu, Y.; Li, G.; Yang, Y. *J. Am. Chem. Soc.* **2014**, *136*, 622−625.
(28) Colella, S.; Mosconi, E.; Fedeli, P.; Listorti, A.; Gazza, F.; Orlandi, F.; Ferro, P.; Besagni, T.; Rizzo, A.; Calestani, G.; Gigli, G.; De Angelis, F.; Mosca, R. *Chem. Mater.* **2013**, *25*, 4613−4618.
(29) Kim, H. B.; Choi, H.; Jeong, J.; Kim, S.; Walker, B.; Song, S.; Kim, J. Y. *Nanoscale* **2014**, *6*, 6679−6683.
(30) Schmidt, L. C.; Pertegas, A.; Gonzalez-Carrero, S.; Malinkiewicz, O.; Agouram, S.; Minguez Espallargas, G.; Bolink, H. J.; Galian, R. E.; Perez-Prieto, J. *J. Am. Chem. Soc.* **2014**, *136*, 850−853.
(31) Mei, A.; Li, X.; Liu, L.; Ku, Z.; Liu, T.; Rong, Y.; Xu, M.; Hu, M.; Chen, J.; Yang, Y.; Gratzel, M.; Han, H. *Science* **2014**, *345*, 295−298.
(32) Zhao, Y.; Zhu, K. *J. Phys. Chem. C* **2014**, *118*, 9412−9418.
(33) Ma, Y.; Zheng, L.; Chung, Y. H.; Chu, S.; Xiao, L.; Chen, Z.; Wang, S.; Qu, B.; Gong, Q.; Wu, Z.; Hou, X. *Chem. Commun.* **2014**, *50*, 12458−12461.
(34) Eperon, G. E.; Burlakov, V. M.; Docampo, P.; Goriely, A.; Snaith, H. J. *Adv. Funct. Mater.* **2014**, *24*, 151−157.
(35) Noh, J. H.; Im, S. H.; Heo, J. H.; Mandal, T. N.; Seok, S. I. *Nano Lett.* **2013**, *13*, 1764−1769.
(36) Momblona, C.; Malinkiewicz, O.; Roldán-Carmona, C.; Soriano, A.; Gil-Escrig, L.; Bandiello, E.; Scheepers, M.; Edri, E.; Bolink, H. J. *Appl. Phys. Lett. Mater.* **2014**, *2*, 081504.
(37) Williams, S. T.; Zuo, F.; Chueh, C. C.; Liao, C. Y.; Liang, P. W.; Jen, A. K. *ACS Nano* **2014**, *8*, 10640−10654.
(38) Stranks, S. D.; Eperon, G. E.; Grancini, G.; Menelaou, C.; Alcocer, M. J.; Leijtens, T.; Herz, L. M.; Petrozza, A.; Snaith, H. J. *Science* **2013**, *342*, 341−344.
(39) Bai, S.; Wu, Z.; Wu, X.; Jin, Y.; Zhao, N.; Chen, Z.; Mei, Q.; Wang, X.; Ye, Z.; Song, T.; Liu, R.; Lee, S.-t.; Sun, B. *Nano. Res.* **2014**, DOI: 10.1007/s12274-014-0534-8.
(40) Etgar, L.; Gao, P.; Xue, Z.; Peng, Q.; Chandiran, A. K.; Liu, B.; Nazeeruddin, M. K.; Gratzel, M. *J. Am. Chem. Soc.* **2012**, *134*, 17396−17179.
(41) Noel, N. K.; Abate, A.; Stranks, S. D.; Parrott, E. S.; Burlakov, V. M.; Goriely, A.; Snaith, H. J. *ACS Nano* **2014**, *8*, 9815−9821.